Systems/Circuits

# Descending Axonal Projections from the Inferior Colliculus Target Nearly All Excitatory and Inhibitory Cell Types of the Dorsal Cochlear Nucleus

**Timothy S. Balmer and Laurence O. Trussell**
Vollum Institute and Oregon Hearing Research Center, Oregon Health & Science University, Portland, Oregon 97239

**The dorsal cochlear nucleus (DCN) integrates auditory nerve input with nonauditory sensory signals and is proposed to function in sound source localization and suppression of self-generated sounds. The DCN also integrates activity from descending auditory pathways, including a particularly large feedback projection from the inferior colliculus (IC), the main ascending target of the DCN. Understanding how these descending feedback signals are integrated into the DCN circuit and what role they play in hearing requires knowing the targeted DCN cell types and their postsynaptic responses. In order to explore these questions, neurons in the DCN that received descending synaptic input from the IC were labeled with a trans-synaptic viral approach in male and female mice, which allowed them to be targeted for whole-cell recording in acute brain slices. We tested their synaptic responses to optogenetic activation of the descending IC projection. Every cell type in the granule cell domain received monosynaptic, glutamatergic input from the IC, indicating that this region, considered an integrator of nonauditory sensory inputs, processes auditory input as well and may have complex and underappreciated roles in hearing. Additionally, we found that DCN cell types outside the granule cell regions also receive descending IC signals, including the principal projection neurons, as well as the neurons that inhibit them, leading to a circuit that may sharpen tuning through feedback excitation and lateral inhibition.**

*Key words:* **auditory; channelrhodopsin; cochlear nucleus; inferior colliculus; midbrain; transsynaptic**

**Significance Statement**

**Auditory processing starts in the cochlea and ascends through the dorsal cochlear nucleus (DCN) to the inferior colliculus (IC) and beyond. Here, we investigated the feedback projection from IC to DCN, whose synaptic targets and roles in auditory processing are unclear. We found that all cell types in the granule cell regions, which process multisensory feedback, also process this descending auditory feedback. Surprisingly, all except one cell type in the entire DCN receive IC input. The IC-DCN projection may therefore modulate the multisensory pathway as well as sharpen tuning and gate auditory signals that are sent to downstream areas. This excitatory feedback loop from DCN to IC and back to DCN could underlie hyperexcitability in DCN, widely considered an etiology of tinnitus.**

## Introduction

The auditory system processes acoustic signals transduced in the cochlea and refined by the neural circuits along the ascending auditory pathway. The cochlear nucleus of the brainstem receives direct input from the auditory nerve and is thus the first, obligate auditory processing region in the brain. Accordingly, the cochlear nucleus is a crucial point in the central auditory pathway where sensory sharpening, modulation, and gating could occur. The dorsal part of the cochlear nucleus (DCN) receives input from nonauditory sources that convey somatosensory, vestibular and proprioceptive signals (Ryugo et al., 2003) for integration with auditory signals for sound source localization or cancellation of self-generated sounds (Singla et al., 2017). In addition to multisensory inputs to DCN, numerous descending inputs from higher-order areas of the auditory system project back to every node in the pathway, potentially providing attentional and contextual information (Kandler et al., 2018). For example, the DCN receives descending auditory input from the superior olivary complex (Faye-Lund, 1986; Benson et al., 1996), primary auditory cortex (Feliciano et al., 1995; Weedman and Ryugo, 1996; Meltzer and Ryugo, 2006), and inferior colliculus (IC; Andersen

Received June 9, 2021; revised Feb. 24, 2022; accepted Feb. 25, 2022.
Author contributions: T.S.B. and L.O.T. designed research; T.S.B. performed research; T.S.B. analyzed data; T.S.B. wrote the first draft of the paper; T.S.B. and L.O.T. edited the paper; T.S.B. and L.O.T. wrote the paper.
This work was supported by National Institutes of Health (NIH) Grants NS028901 and DC004450 (to L.O.T.), K99 DC016905 (to T.S.B.), P30 DC005983, and P30 NS0618000. We thank Dr. Pierre Apostolides for comments on the manuscript.
T. S. Balmer's present address: School of Life Sciences, Arizona State University, Tempe, Arizona 85281.
The authors declare no competing financial interests.
Correspondence should be addressed to Laurence O. Trussell at trussell@ohsu.edu.
https://doi.org/10.1523/JNEUROSCI.1190-21.2022
Copyright © 2022 the authors

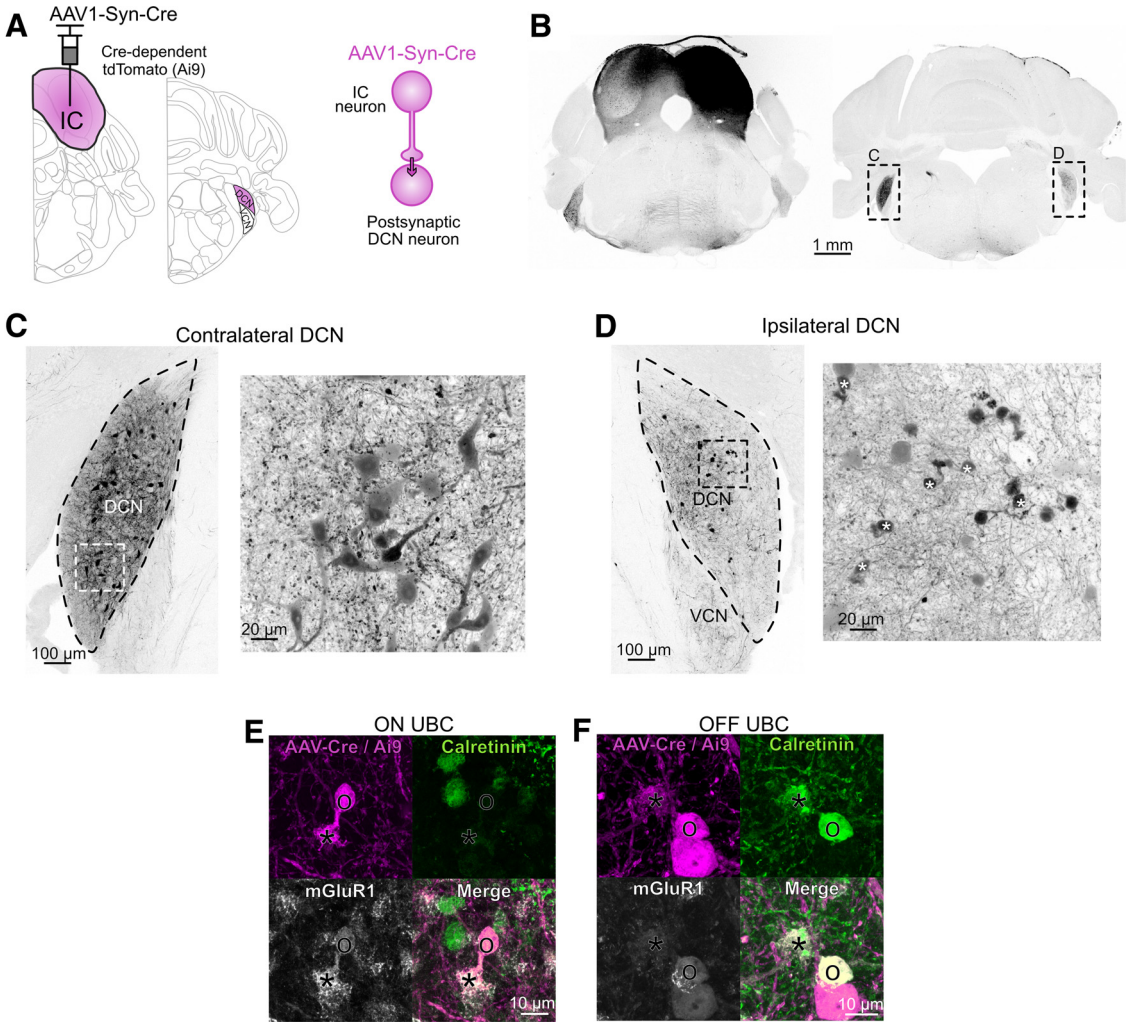


**Figure 1.** Anterograde trans-synaptic labeling of DCN neurons. ***A***, Diagram showing viral approach to label neurons in DCN that receive axonal input from IC. The AAV1-Syn-Cre virus is injected into IC of the Cre-dependent reporter mouse line (Ai9). The infected IC neurons transmit the virus to postsynaptic neurons in DCN, which drives tdTomato expression. ***B***, Brain sections showing injection into right IC, which causes tdTomato expression (black) in local neurons as well as postsynaptic neurons in the ipsilateral DCN. Note that numerous neurons in the contralateral DCN are also labeled, owing to the ability of this virus to infect axons and thereby labeling the major projection from the contralateral T-stellate cells of the VCN and the fusiform and giant cells of the DCN. ***C***, Left, DCN contralateral to the injected IC. Many large cells and their processes are labeled. Right, Magnified view of boxed region. Large cells that are most likely fusiform and giant cells are presumed to be retrogradely labeled by direct infection of their axons at the injection site in IC. Z-projection. ***D***, Left, DCN ipsilateral to the injected IC has numerous labeled neurons and their processes, as well as the descending IC axons. There are fibers in the VCN, but no labeled somata, which suggests that these fibers are those of neurons postsynaptic to the targets of IC, such as vertical cells. Right, Magnified view of boxed region. Many UBCs (*) and granule cells are labeled, as are larger cells that may be Golgi or vertical cells. These cells have not been reported to project their axons outside of DCN and could therefore not have been retrogradely-labeled and were instead labeled trans-synaptically via the descending axons. Z-projection. ***E***, Trans-synaptically labeled UBC (magenta) was co-labeled with mGluR1 (white) but not calretinin (green). This is therefore an ON UBC. Note that the mGluR1 labeling is in the brush. (The labeling in the soma is likely bleed-through from the red channel.) Soma marked with O, brush marked with *. Z-projection. ***F***, Trans-synaptically labeled UBC (magenta) that was co-labeled with calretinin (green) but not mGluR1 on the brush (white). This is therefore an OFF UBC. Soma marked with O, brush marked with *. Z-projection.

et al., 1980; Conlee and Kane, 1982; Caicedo and Herbert, 1993; Malmierca et al., 1996; Schofield, 2002). The targets of descending auditory input in DCN are unknown and must be clarified to address their role in hearing. Moreover, knowing the nature of their synaptic responses is necessary to identify whether they act, for example, to modulate the synapses by releasing neuromodulators, or to drive or suppress the activity of postsynaptic cells by releasing neurotransmitters.

The IC, which is the primary target of the projections from DCN, sends signals back to DCN that have been inferred to be glutamatergic based on anatomical data (Milinkeviciute et al., 2017). The cell types in the granule cell region that surrounds DCN include granule cells, Golgi cells, and unipolar brush cells (UBCs) and presumably these integrate extrinsic multisensory (nonauditory) signals. While it might be expected that this region conveys all nonauditory nerve input to DCN principal cells, anatomical data shows that the descending IC projection terminates across the deep layers of the DCN (Milinkeviciute et al., 2017), which contains numerous UBCs, but also a number of other cell types that receive direct input from the auditory nerve and are not thought to receive descending sensory input. Our goal was to identify which cell types across the entire DCN receive descending input from IC and test their postsynaptic responses to address whether they are indeed glutamatergic and whether they are capable of driving action potential firing.

This is a difficult question to address because of the numerous intermingling axonal projections to DCN from diverse and unclear sources. An optogenetic approach was used to target the light-gated ion channel Channelrhodopsin-2 (ChR2) to axons projecting to neurons in DCN, so that they could be activated

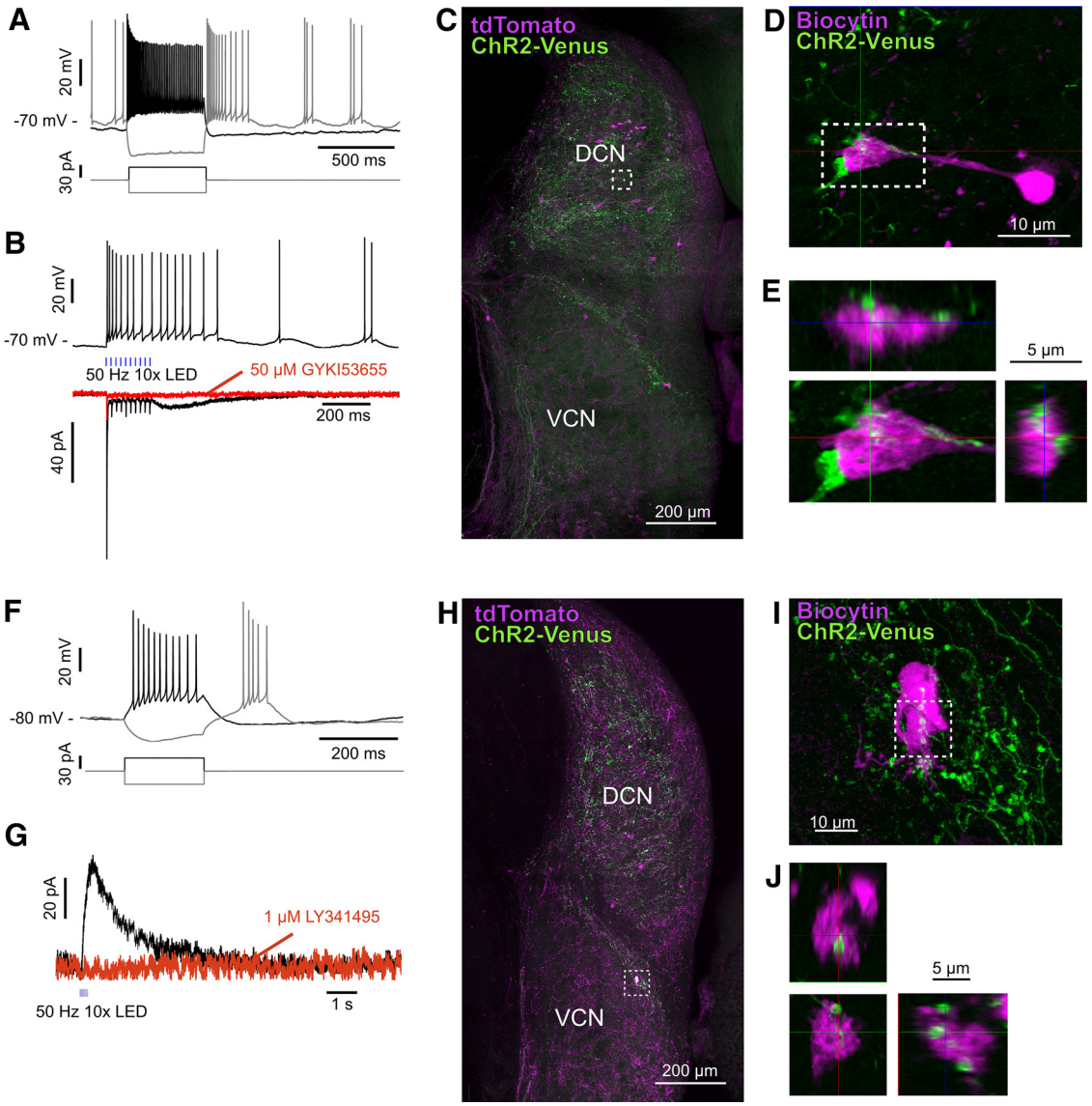


**Figure 2.** Glutamatergic descending IC projections synapse onto ON and OFF UBCs. ***A***, 30-pA hyperpolarizing and depolarizing current steps. Depolarization evoked spikes that decreased in amplitude, diagnostic of UBCs. ***B***, Top, 50-Hz ChR2 stimulation evoked an increase in spiking that outlasted the duration of stimulation. Bottom, 50-Hz ChR2 stimulation evoked fast EPSCs that depressed, followed by a slow inward current that was blocked by GYKI53655 (red) and was therefore mediated by AMPARs. The latency of the first EPSC was 1.87 ms on average. These synaptic currents were recorded in the presence of 50 $\mu$M 4-AP. ***C***, This ON UBC was recovered after amplifying tdTomato and Venus with antibodies for super-resolution imaging. Note the trans-synaptically labeled cells and processes (magenta) and descending IC axons (green). Z-projection. ***D***, Magnified view of boxed region in ***C***. Biocytin-labeled UBC. Single optical section. ***E***, Magnified region in ***D*** with orthogonal views from the z-stack. The descending ChR2-expressing axon (green) clearly contacts the dendritic brush of the ON UBC. Five ON UBCs with ChR2-evoked monosynaptic input have been recovered from three mice. ***F***, 30-pA hyperpolarizing and depolarizing currents steps evoked spikes that decreased in amplitude, diagnostic of UBCs. ***G***, 50-Hz ChR2 stimulation evoked a slow IPSC that was mediated by mGluR2 receptors and is diagnostic of an OFF UBC. Recorded in the presence of 50 $\mu$M 4-AP. ***H***, This OFF UBC was in the granule cell domain between DCN and VCN. Z-projection. ***I***, Magnified view of boxed region in ***H***. Biocytin-labeled UBC. Z-projection. ***J***, Single optical section of the boxed region in ***I*** with side views of the z-stack. Note the many locations that the IC axon (green) contacts the dendritic brush of the OFF UBC. Two OFF UBCs with ChR2-evoked monosynaptic input were characterized from two mice.

specifically in acute brain slices. Finding individual neurons that receive monosynaptic input from a specific source is challenging, especially for relatively small projections and for cells that receive few inputs, such as granule cells and UBCs. To target whole-cell recordings to DCN neurons that received IC input, we used a trans-synaptic virus approach that fluorescently labeled neurons that received direct (monosynaptic) axonal input from IC neurons (Zingg et al., 2017, 2020). As predicted, granule cells, UBCs, and Golgi cells received direct, glutamatergic input from IC. In addition, we discovered that numerous other cell types process this input, suggesting that the IC is a strong source of top-down control of the first auditory processing region in the brain that may sharpen tuning, improve feature detection, and underlie other complex functions. This anatomically defined, feedback loop from DCN to IC and back to DCN could sustain the hyperexcitability in the DCN that is considered an etiology of tinnitus.

## Materials and Methods

### *Animals*

Ai9(RCL-tdT) (Madisen et al., 2012) or C57BL/6J mice were bred in a colony maintained in the animal facility managed by the Department of

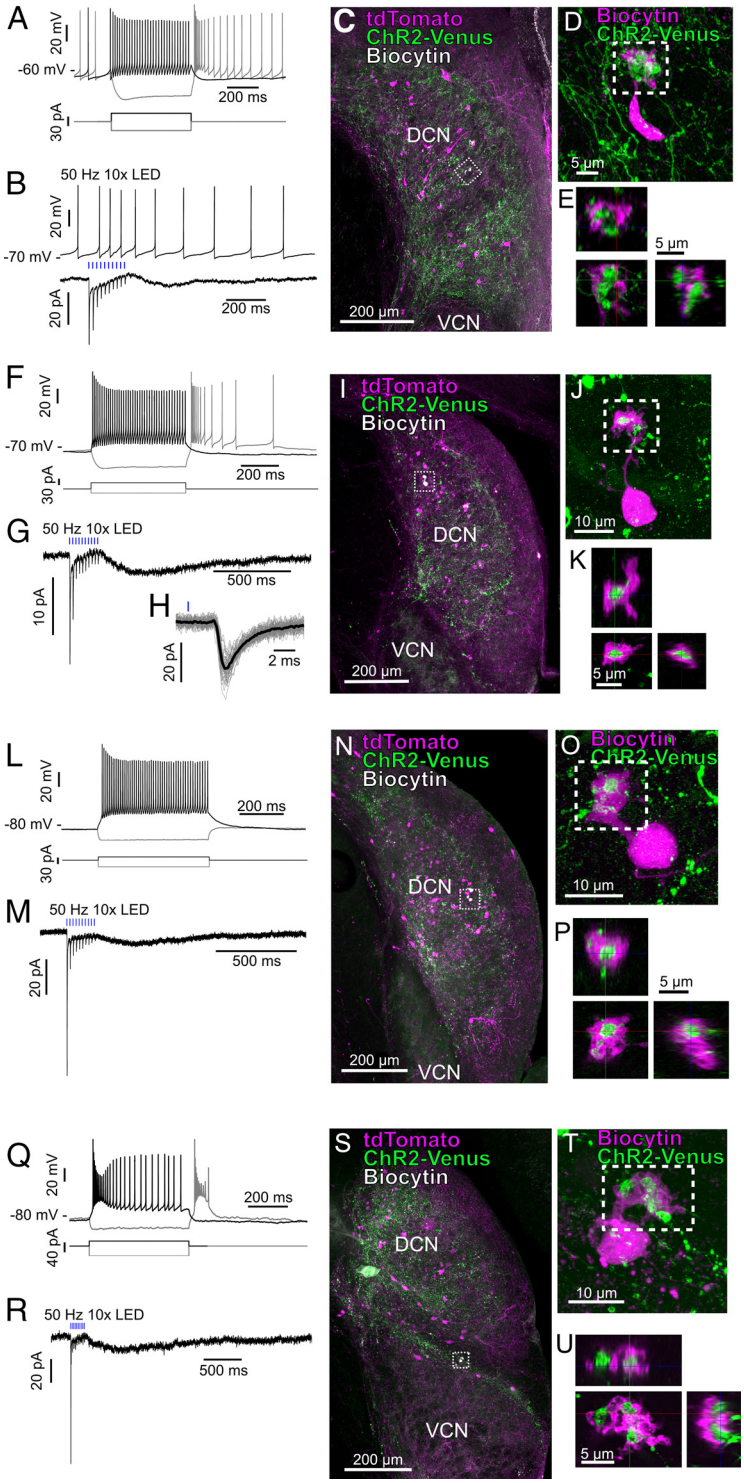


**Figure 3.** Additional examples of UBCs with anatomically and functionally defined connections. ***A***, Depolarizing and hyperpolarizing current pulses elicited responses typical of ON UBCs. ***B***, 50-Hz LED train increased the firing rate of the UBC in current clamp mode (top) and evoked currents that identified this cell as an ON UBC in voltage clamp mode (bottom). The average latency of the first EPSC was 1.72 ms, and there were no failures. The response to the LED train in current clamp mode was done before application of 4-AP. The currents were recorded in the presence of 50 $\mu$M 4-AP. ***C***, During whole-cell recording, the UBC whose responses are shown in ***A***, ***B*** was filled with biocytin and recovered for anatomic analysis. Z-projection. ***D***, A large mossy fiber axon terminal labeled with ChR2-Venus contacted the UBC's brush. The soma of this UBC was damaged by the removal of the patch pipette. Z-projection. ***E***, Orthogonal views of the boxed region in ***D***. Single optical planes. ***A–E*** data from same cell. ***F***, Typical ON UBC response to depolarizing and hyperpolarizing current pulses. ***G***, 50-Hz LED train evoked currents diagnostic of an ON UBC: phasic EPSCs that depress, followed by a EPSC beginning at the end of stimulation. These currents were recorded in the presence of 50 $\mu$M 4-AP. ***H***, EPSPs evoked by 0.1-ms LED. The average latency of these EPSCs was 2.70 ms, and there were no failures. The currents were recorded in the presence of 50 $\mu$M 4-AP. ***I***, This UBC was found in the deep layer of DCN. Z-projection. ***J***, The mossy fiber terminal (green) is virtually surrounded by the dendrite of the biocytin-filled UBC. Z-projection. ***K***, Orthogonal views of boxed region in ***J***. Single optical planes. ***F–K*** data from same cell. ***L***, Response to depolarizing and hyperpolarizing current steps. ***M***, 50-Hz train of 5-ms LED light pulses evoked a current response diagnostic of an ON UBC. The average latency of the EPSCs was 2.59 ms, and there were no failures. These currents were recorded in the presence of 50 $\mu$M 4-AP. ***N***, This ON UBC was also recovered in the deep layer of DCN. Z-projection. ***O***, Expanded view of boxed region in ***N***. Z-projection. ***P***, Orthogonal views of boxed region in ***O***. Single optical planes. ***L–P*** data from same cell. ***Q***, Response to depolarizing and hyperpolarizing current steps. ***R***, 50-Hz train of 5-ms LED light pulses evoked a current response diagnostic of ON UBCs. The average latency of the EPSCs was 2.48 ms, and there were no failures. These currents were recorded in the presence of 50 $\mu$M 4-AP. ***S***, This UBC was in the granule cell region between DCN and VCN. Z-projection. ***T***, Expanded view of boxed region in ***S***. Z-projection. ***U***, Orthogonal views of boxed region in ***T***. Single optical planes. ***Q–U*** data from same cell.

Comparative Medicine and all procedures were approved by the Oregon Health and Science University's Institutional Animal Care and Use Committee. Mice had access to food and water *ad libitum* and were kept on a 12/12 h light/dark cycle.

*Brain slice preparation*

Animals were anesthetized with isoflurane, decapitated, and the brain was dissected from the skull under ice-cold high-sucrose artificial CSF (ACSF) solution containing the following (in mM): 87 NaCl, 75 sucrose, 25 $NaHCO_3$, 25 glucose, 2.5 KCl, 1.25 $NaH_2PO_4$, 0.4 Na-ascorbate, 2 Na-pyruvate, 0.5 $CaCl_2$, and 7 $MgCl_2$, bubbled with 5% $CO_2$/95% $O_2$. In some experiments 5 $\mu$M MK-801 was included in high-sucrose ACSF. Coronal brainstem sections 200 $\mu$m thick were cut with a vibratome (7000smz-2, Campden Instruments) in ice-cold high-sucrose ACSF. Slices recovered at 35°C for 30–40 min, in recording ACSF containing the following (in mM): 130 NaCl, 2.1 KCl, 1.2 $KH_2PO_4$, 3 Na-HEPES, 10 glucose, 20 $NaHCO_3$, 0.4 Na-ascorbate, 2 Na-pyruvate, 1.2–2.0 $CaCl_2$, 1 $MgSO_4$, and 0.005 MK-801, bubbled with 5% $CO_2$/95% $O_2$ (300–305 mOsm). Slices were kept at room temperature (~23°C) until recording. MK-801 was maintained in the ACSF as it appeared to preserve the health of the UBCs in these recordings.

*Electrophysiological recordings*

All electrophysiological experiments were performed 6–18 d after viral injection. Acute brain slices were prepared from males and females, postnatal day (P)27–P40. During recordings, slices were perfused with recording ACSF using a peristaltic pump (Ismatec) at 3 ml/min, and maintained at ~34°C with an inline heater (Warner Instruments). Slices were viewed on a fixed-stage microscope (Zeiss) using an infrared Dodt contrast mask, a 60× objective (Olympus) and camera (Dage-MTI). Patch electrodes were pulled with borosilicate glass capillaries (OD 1.2 mm and ID 0.68 mm, World Precision Instruments) with an upright puller (PC10, Narishige). Intracellular recording solution contained (mM): 113 K-gluconate, 9 HEPES, 4.5 $MgCl_2$, 0.1 EGTA, 14 Tris-phosphocreatine, 4 $Na_2$-ATP, 0.3 tris-GTP, and 0.1–0.3% biocytin (adjusted to 290 mOsm with sucrose), pH 7.2–7.25. All recordings were corrected for a −10 mV junction potential. For data acquisition we used a Multiclamp 700B amplifier and pClamp 9

**Table 1. Parameters for IC-evoked synaptic responses in DCN cell types**

| Cell type | Amplitude (pA) | Latency (ms) | Jitter (SD of latency, ms) | Success rate (successes/trials) | Number of cells |
|---|---|---|---|---|---|
| Granule | −76.1 ± 94.0* | 3.22 ± 0.95 | 0.23 ± 0.14 | 0.84 ± 0.26 | 9 |
| ON UBC | −73.1 ± 34.0 | 2.27 ± 0.45 | 0.09 ± 0.05 | 1 ± 0 | 4 |
| Golgi | −47.4 | 1.54 | 0.14 | 0.87 | 1 |
| Principal | −54.4 ± 26.2 | 2.92 ± 0.60 | 0.33 ± 0.14 | 0.94 ± 0.14 | 5** |
| Vertical | −115.2 ± 53.6 | 2.39 ± 0.91 | 0.17 ± 0.09 | 0.91 ± 0.11 | 9 |
| Cartwheel | −100.9 ± 96.1 | 3.55 ± 2.58 | 0.29 ± 0.11 | 0.79 ± 0.28 | 3 |

*means given ±SD.
**One additional fusiform cell was responsive but had too many spontaneous events to enable an accurate measurement.

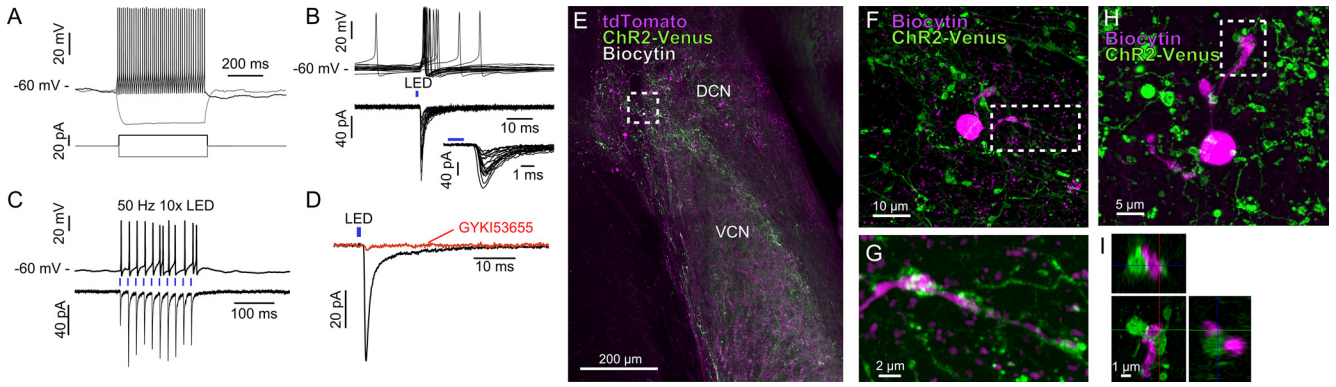


**Figure 4.** Descending IC projections target granule cells. ***A***, Current clamp recording of a granule cell. 20-pA hyperpolarizing and depolarizing currents steps. Note the high input resistance, diagnostic of granule cells. ***B***, A single 1-ms flash of light was sufficient to trigger action potentials in current clamp and evoke EPSCs of various amplitudes with low jitter in voltage clamp. Inset shows the evoked currents with an expanded time base. ***C***, 50-Hz train of light pulses evoked at least one spike on each pulse coinciding with evoked currents. ***D***, The synaptic current was blocked by 50 $\mu$M GYKI53655 and was therefore mediated by AMPARs. ***E***, This cell was in the granule cell domain between DCN and VCN. Z-projection. ***F***, Magnified view of boxed region in ***E***. Biocytin-labeled granule cell. Z-projection. ***G***, Magnified view of boxed region in ***E***. The IC axon (green) contacts the dendrite of the granule cell in several locations. Z-projection. ***H***, Another example of a granule cell that was recovered after whole-cell recording. Z-projection. ***I***, Magnified view of boxed region in ***H*** showing synaptic contacts between the green IC axons and the magenta dendritic claw. Single optical section. The top and side panels show side views of the image stack.

software (Molecular Devices). Signals were sampled at 20–50 kHz using a Digidata (1440A, Molecular Devices) analog-digital converter. Current signals in voltage clamp were acquired with 5–10× gain and low-pass filtered at 10 kHz, with further digital filtering applied offline. Patch pipettes tip resistance was 6–8 MΩ; series resistance was compensated with correction 20–40% and prediction 50–70%, bandwidth 2 kHz. Membrane potential was held constant at −70 mV in voltage clamp recordings. ChR2 was activated using full-field blue LED light flashes (Sutter or Thor Labs) through a GFP filter set. In some cases in which the synaptic response reliability was low, 50 $\mu$M of the $K^+$ channel blocker 4-aminopyridine (4-AP) was used to increase the reliability of ChR2-evoked transmitter release, presumably by lowering spike threshold and increasing spike width. Latency was measured from the beginning of the LED pulse to the commencement of the EPSC. The time of the commencement of the EPSC (the foot) was calculated as the intersection between the baseline and an extrapolation of a line through the points at which the rising phase of the EPSC reached 20% and 80%, using StimFit (Guzman et al., 2014). Reliability rate was calculated as the number of LED flashes that evoked an EPSC divided by the number of trials.

The descending IC inputs were determined to be monosynaptic using three different approaches: (1) the monosynaptic transfer of the virus into the cell that was targeted for recording; (2) the physiological characteristics of the ChR2 evoked current; (3) in many cases the recorded cells were imaged for an anatomical verification of ChR2-Venus-labeled fibers apposing the recorded cell's dendrite. Any one of these approaches is a standard for determining monosynaptic input. In this study the first two approaches were used for all cells and the anatomical connection was verified in nearly all of the 32 cells recorded; 19 of these connections are illustrated here. Monosynaptic currents were differentiated from polysynaptic currents by their short latencies (2.77 ± 1.10 ms, $n = 32$, mean ± SD), low jitter (0.21 ± 0.13 ms, $n = 32$, mean ± SD), reliability (0.90 ± 0.18, i.e., 90% of LED flashes evoked an EPSC, $n = 32$, mean ± SD). This is well within the latencies seen in similar preparations where monosynaptic currents were characterized (Petreanu et al., 2007, 2009).

*Viral injections*

Viral injections were made into the IC in P21–P25 mice using a stereotax (Kopf), single axis manipulator (Narishige) and pipette vice (Ronal) under isoflurane anesthesia. Glass capillaries (Drummond Scientific) were pulled on a pipette puller (Sutter) and beveled at 45° angle with a 20- to 30-µm inside diameter using a diamond lapping disk (3M). An incision was made in the scalp along the midline and a small hole was drilled into the skull. The pipette was lowered into the brain at 10 µm/s. Five-minute periods were allowed before and after injection; 50–300 nl of virus was injected using stereotaxic coordinates (5.5 mm caudal, 1.1 mm lateral, 1.0 mm ventral, relative to bregma). AAV1-Syn-Cre (3.15e13 GC/ml, U Penn), AAV1-CAG-ChR2-Venus (8.99e12 GC/ml, U Penn) were injected alone or mixed 1:1 by volume and injected together. AAV1-Chronos-GFP (1.4e13 GC/ml, Addgene) was used instead of the ChR2-Venus virus in a single experiment that yielded ChR2-evoked EPSCs in one granule cell and one Golgi cell. We did not differentiate whether the injection site included the central nucleus or the lateral/external cortex of the IC, because previous work in the mouse showed that all major subdivision of the IC project to DCN (Milinkeviciute et al., 2017).

*Immunohistochemistry and imaging*

Mice were overdosed with isoflurane and perfused through the heart with 0.01 M PBS, 7.4 pH followed by 4% paraformaldehyde in PBS. Brains were extracted from the skull and incubated in 4% paraformaldehyde in PBS overnight at 4°C. Brains were transferred to 30% sucrose in PBS for >2 d; 50-µm-thick sections were made on a cryostat (Microm) at ~22°C and saved as floating sections in PBS. When labeling mGluR1

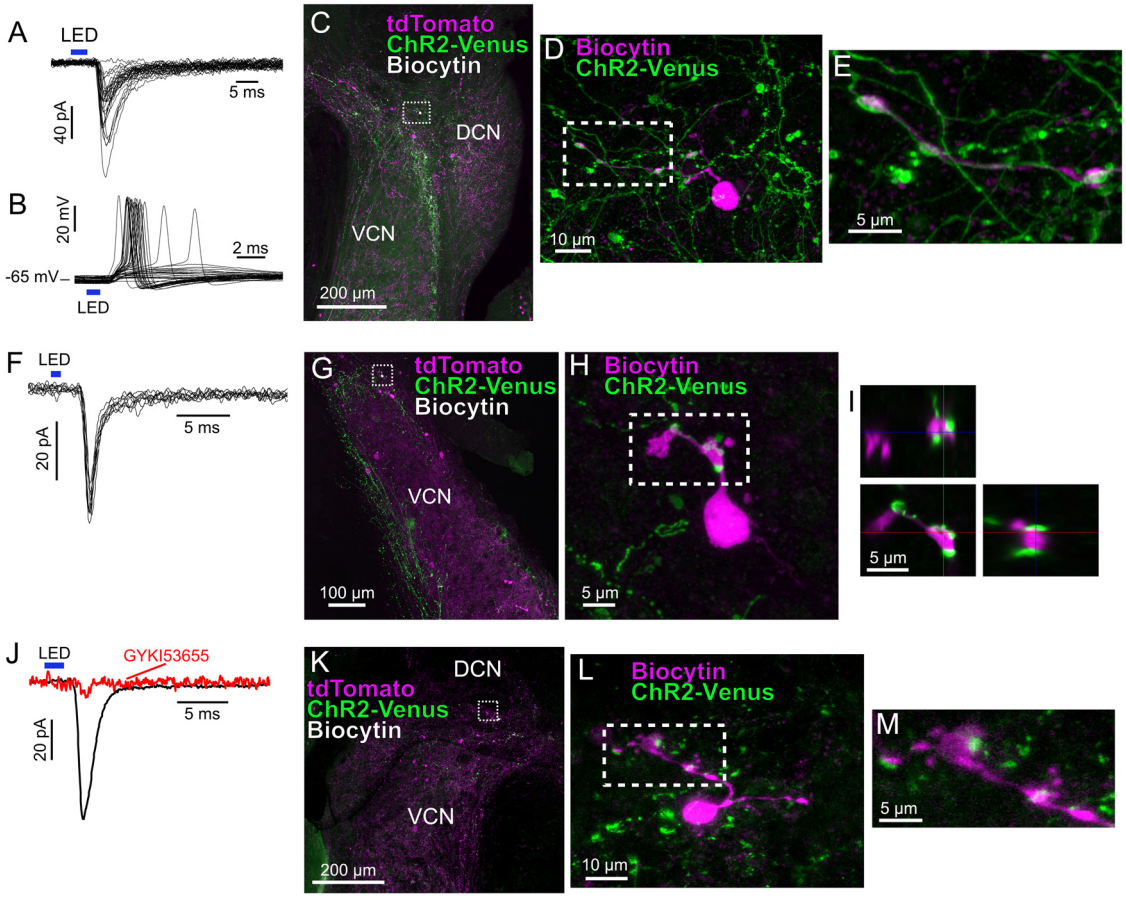


**Figure 5.** Three additional examples of granule cells with anatomically and functionally defined connections from IC. ***A***, In this granule cell, LED-evoked EPSCs varied in amplitude, perhaps because of multiple synapses. Note that there was only one failure in this series of LED flashes. ***B***, LED flashes evoked single spikes in most trials. ***C***, The granule cell recorded in ***A***, ***B*** was found between DCN and VCN. ***D***, This cell had a relatively long dendrite receiving multiple axonal contacts. Z-projection. ***E***, Expanded view of boxed region in ***D***. Z-projection. ***F***, LED-evoked EPSCs with an average latency of 3.79 ms and no failures. 50 $\mu$M 4-AP was present in this experiment. ***G***, This example was also recovered and was in the region between DCN and VCN. ***H***, The filled granule cell had two dendrites (one is directly below the soma). One of the dendrites received multiple bouton-like contacts from a ChR2-Venus-labeled fiber. Z-projection. ***I***, Orthogonal views of the boxed region in ***H***. Single optical planes. ***J***, In this example granule cell, LED-evoked EPSCs had an average latency of 3.43 ms, no failures, and were blocked by AMPA receptor antagonist GYKI53655 (50 $\mu$M). 50 $\mu$M 4-AP was present in this experiment. ***K***, The granule cell was located in the region between DCN and VCN. ***L***, This granule cell had multiple dendrites, one of which received ChR2-Venus-labeled axonal input. Z-projection. ***M***, Expanded view of boxed region in ***L***. Z-projection.

and calretinin, brains were transferred to PBS instead of 30% sucrose and sectioned on a vibratome (Leica). To recover cells that were filled with biocytin during whole-cell recording, acute brain slices were fixed overnight in 4% paraformaldehyde in PBS, followed by storage in PBS. Both floating 50-µm sections and 300-µm-thick acute slices were treated with the following procedures. Sections were rinsed 3 × 10 min in PBS, blocked and permeabilized in 2% BSA, 2% fish gelatin, 0.2% Triton X-100 in PBS for >2 h at room temperature. Primary antibodies were diluted in 1% fish gelatin in PBS and included rabbit anti-calretinin (1:2000, Swant 7697), chicken anti-GFP (1:2000, Aves Labs GFP-1020), goat anti-mCherry (1:2000, Sicgen AB0040-200), mouse anti-mGluR1a (1:800 BD Pharmingen 556389). Sections were incubated in primary antibodies for 2–3 d at 4°C on an orbital shaker. Sections were rinsed 3 × 10 min in PBS, followed by secondary antibodies and streptavidin for 2–3 d at 4°C on an orbital shaker. Secondary antibodies were diluted 1:500 in 1% fish gelatin in PBS and included donkey anti-rabbit Alexa Fluor 488 (Jackson ImmunoResearch, 711-545-152), donkey anti-chicken Alexa Fluor 488 (Jackson ImmunoResearch, 711-165-150), donkey anti-goat Cy3 (Jackson ImmunoResearch, 705-165-147), and donkey anti-mouse Alexa Fluor 647 (Jackson ImmunoResearch, 715-605-151. Alexa Fluor 647 conjugated streptavidin was included in the secondary antibody cocktail to label biocytin-filled cells (1:2500, ThermoFisher Scientific S21374). Sections were mounted on microscope slides and coverslipped with CFM-3 (CitiFluor). Images were acquired on a confocal microscope (Zeiss 780 or 880) or on a Zeiss Elyra PS.1 with AiryScan system that reconstructs super-resolution images from a series of images acquired under spatially structured illumination (Gustafsson, 2000).

## Results

### Anterograde trans-synaptic labeling of DCN neurons that receive input from IC

To test the hypothesis that fibers from IC drive cells in the granule cell domain, the identity of those cells must be determined. We focused on the ipsilateral IC-DCN projection because it is much larger than the contralateral projection (Milinkeviciute et al., 2017). We injected a Cre-recombinase (Cre) expressing adeno-associated virus (AAV1-Syn-Cre) into the right IC of Ai9 reporter mice that express the red fluorescent protein tdTomato in cells that contain Cre (Fig. 1*A*). This injection caused expression of tdTomato in numerous neurons in the right IC (Fig. 1*B*). The AAV1-Syn-Cre virus has been validated as a monosynaptic anterograde tracer, because of its ability to jump from the neurons that are initially infected at the injection site into postsynaptic neurons, causing the expression of Cre-dependent transgenes (Zingg et al., 2017, 2020). As expected, numerous neurons in the ipsilateral DCN expressed tdTomato, indicating that Cre was transmitted from descending axons to their postsynaptic targets

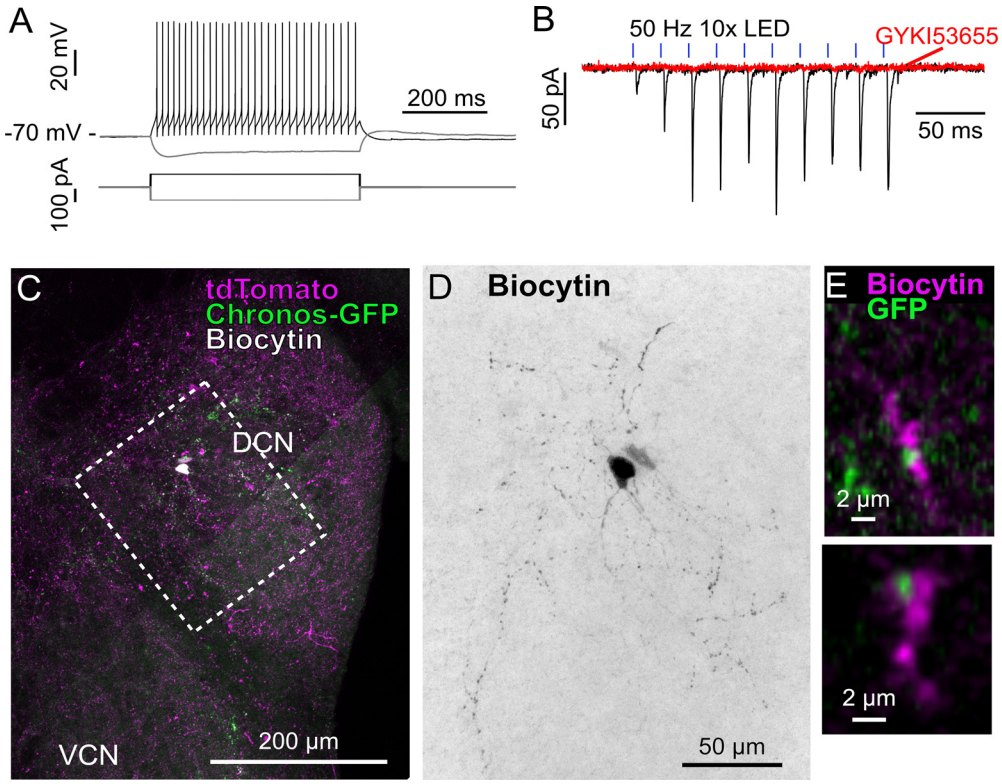


**Figure 6.** Inhibitory Golgi cell receives descending input from IC. ***A***, Current clamp recording of a Golgi cell. 100-pA hyperpolarizing and depolarizing currents steps. Note the low input resistance compared with UBCs and granule cells. ***B***, 50-Hz ChR2 stimulation evoked EPSCs that facilitated that were mediated by AMPARs, consistent with Golgi cell responses to synaptic input. ***C***, This cell was in the deep layer of DCN. ***D***, Magnified view of boxed region in ***C***. Biocytin-labeled Golgi cell. Z-projection. The less brightly labeled cell may have been filled with biocytin indirectly via gap junctions that are known to connect Golgi cells. ***E***, Examples of contacts between Chronos-GFP-labeled fibers and biocytin-labeled dendrite. Single optical planes.

(Fig. 1*D*). The cell bodies of the labeled neurons varied in size from very small (<8 µm, presumably granule cells), and intermediate sizes (8–10 µm, presumably UBCs), but also much larger neurons that could be Golgi cells, in addition to several cell types not found in the granule cell domain, as described below. The DCN contralateral to the injection site contained labeled cells that are presumed to be fusiform and giant cells (Fig. 1*C*), because (1) fusiform and giant cells send their axons to the contralateral IC and (2) the virus we used can infect axons directly. We did not explore the contralateral projection from IC to DCN further and instead focused on the much larger projection from the IC to the ipsilateral DCN.

### UBCs receive descending input from IC

Some cell types in the DCN can be identified by their morphology. UBCs, for example, have a characteristic single dendritic brush and a soma of ~10 µm in diameter. Numerous UBCs were labeled in the deep layer of DCN (Fig. 1*D*). There are two major subtypes of UBCs, ON and OFF UBCs, named for their excitatory and inhibitory response to glutamate (Borges-Merjane and Trussell, 2015). ON and OFF UBCs can be identified by their expression of either mGluR1 in ON UBCs or calretinin in OFF UBCs (Borges-Merjane and Trussell, 2015). Immunohistochemical labeling of the trans-synaptically labeled UBCs revealed that both UBC subtypes were targets of the descending IC projection (Fig. 1*E*,*F*).

This descending IC projection has the anatomical characteristics of excitatory synapses (Milinkeviciute et al., 2017), although postsynaptic responses have not been confirmed. To directly address the synaptic responses of the targets of this projection, we combined the trans-synaptic labeling approach with optogenetics. A virus expressing the light-gated ion channel ChR2 and a green fluorophore (Venus; AAV1-CAG-ChR2-Venus) was co-injected into IC with the cre-expressing virus. One to two weeks after injection, acute brain slices were prepared and tdTomato-expressing cells were targeted for whole-cell recording. In most cases, after characterizing the cell and its responses in current clamp, a low concentration of the nonspecific K-channel blocker 4-AP (50 $\mu$M) was added to increase the reliability of ChR2-evoked neurotransmitter release, which assisted in the characterization of the postsynaptic currents.

Figure 2*A*,*B* shows an example recording from a tdTomato-expressing UBC. In these images, tdTomato is shown in magenta. UBCs can be identified electrophysiologically by their prominent spike-height adaptation (Fig. 2*A*). A train of light flashes was used to activate the ChR2-expressing descending fibers, which evoked synaptic currents consistent with the ON UBC response- phasic EPSCs that depress, followed by a rebound EPSC at the end of stimulation (Fig. 2*B*; Rossi et al., 1995). The latency from the beginning of the light pulse to the beginning of the EPSC was 2.27 ± 0.45 ms (mean ± SD) and in all five ON UBCs the pulse never failed to elicit an EPSC. Out of four ON UBCs that received IC input that could be resolved without the addition of 4-AP, three fired action potentials in response to a single light pulse (0.1–5 ms), while one additional ON UBC required a train of light pulses to fire. In all cases tested, the EPSCs were almost completely blocked by AMPAR antagonist GYKI53655 [50 $\mu$M, 87.44 ± 0.05% blocked (mean ± SD), $n = 3$ ON UBCs; Fig. 2*B*]. The UBC shown in Figure 2*A*,*B* was filled with biocytin and imaged on a super-resolution microscope to verify the cell's location and morphology, and to visualize the

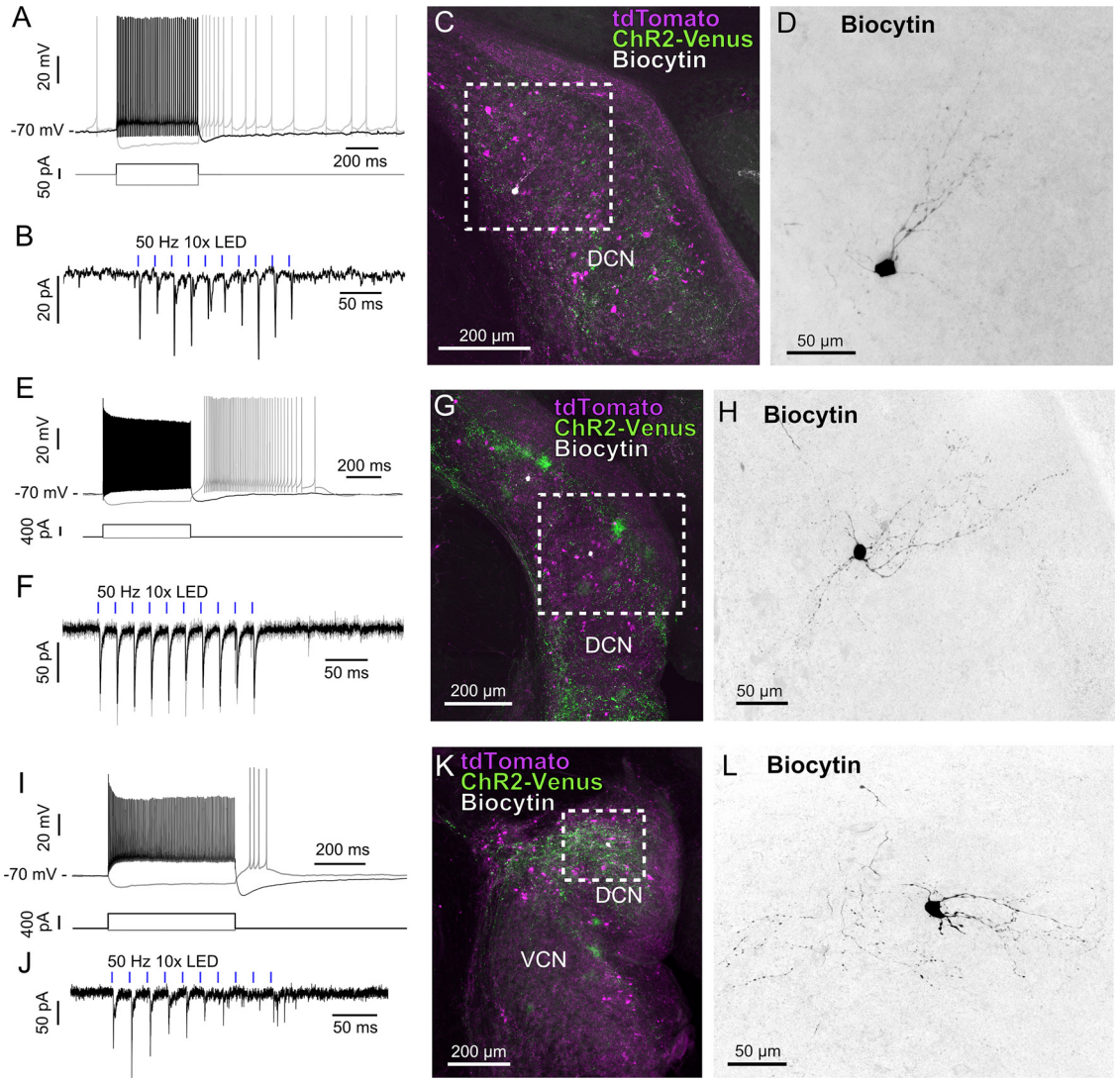


**Figure 7.** Vertical cells receive descending IC input. ***A***, Current clamp recording of a vertical cell. 50-pA hyperpolarizing and depolarizing currents steps. Note the characteristic high firing rate. ***B***, 50-Hz ChR2 stimulation evoked fast monosynaptic and polysynaptic EPSCs. Recorded in the presence of 50 $\mu$M 4-AP. ***C***, This cell was in the deep layer of DCN and had a narrow dendritic arbor that extended dorsally. Z-projection. ***D***, Magnified view of boxed region in ***C***. Biocytin-labeled vertical cell. Z-projection. ***E***, Hyperpolarizing current step caused rebound firing (gray) and depolarizing step caused high-frequency spiking up to 430 Hz, consistent with a vertical cell identification. ***F***, 50-Hz train of light pulses evoked fast EPSCs. The latency to the foot of the first EPSC was 1.53 ms on average. Gray traces are single trials and black trace is average. These currents were recorded in the presence of 50 $\mu$M 4-AP. ***G***, Example of a vertical cell that was filled with biocytin during whole-cell recording. Z-projection. ***H***, Expanded view of boxed region in ***G***. Z-projection. ***I***, Hyperpolarizing current step caused rebound firing (gray) and depolarizing step caused high-frequency spiking up to 278 Hz, consistent with a vertical cell identity. ***J***, 50-Hz train of light pulses evoked fast EPSCs. The latency to the foot of the first EPSC was 2.00 ms on average. These currents were recorded in the presence of 50 $\mu$M 4-AP. ***K***, Image of the area of DCN containing the vertical cell that was filled with biocytin during whole-cell recording shown in ***I***, ***J***. ***L***, Expanded view of boxed region in ***K***.

synaptic contact (Fig. 2*C–E*). ChR2-Venus expressing (green) descending IC axons are present in the DCN deep layers and the granule cell regions, but not the molecular layer. tdTomato-expressing (magenta) fibers are present in all regions including the molecular layer and include both descending axons (some of which are also green) and the trans-synaptically labeled cells; the magenta fibers in the molecular layer are most likely trans-synaptically labeled parallel fibers of granule cells. The UBC whose synaptic responses are shown in Figure 2*A*,*B* was in the deep layer, where UBCs are present in highest density (Fig. 2*C*). Notably, the axon seen making contact with the UBC dendrite appeared smaller than the typical mossy fibers that innervate ON UBCs in the cerebellum (Balmer and Trussell, 2019). Four additional examples of ON UBCs and their input from IC are provided in Figure 3; they confirm that the IC input occupies only a portion for the large brush dendrite, despite producing substantial synaptic responses. Altogether, these examples suggest that at least some, and perhaps most, of the synaptic responses described for UBCs in DCN may have originated from the IC (Borges-Merjane and Trussell, 2015). Table 1 gives parameters (amplitude, latency, jitter, reliability) for optogenetically-evoked synaptic responses in this study.

Descending glutamatergic projections evoked outward currents in two OFF UBCs. In the example shown in Figure 2*F–J*, optogenetic activation of descending axons caused an outward current that was blocked by mGluR2 antagonist LY341495 (1 $\mu$M), characteristic of the OFF UBC response to glutamate (Borges-Merjane and Trussell, 2015). This OFF UBC was in the granule cell region between DCN and VCN. Because mGluR2-

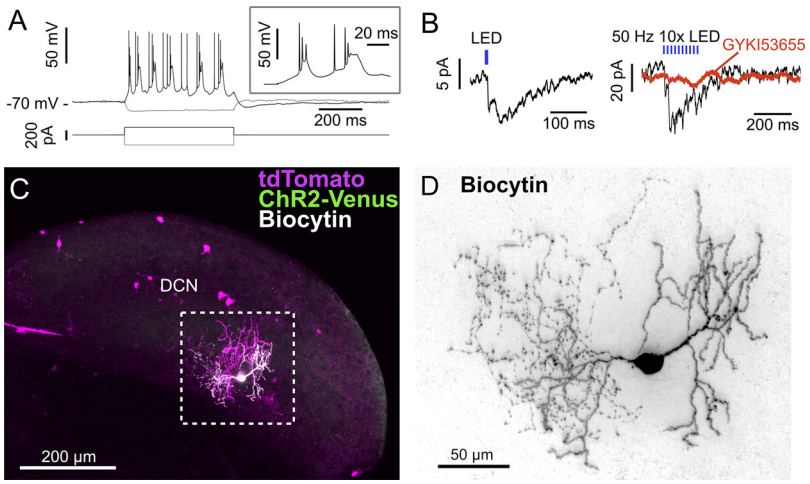


**Figure 8.** Cartwheel cells receive descending IC input. ***A***, Hyperpolarizing and depolarizing currents steps, the latter evoking complex spikes diagnostic of cartwheel cells. Expanded time base in inset shows complex spiking pattern. ***B***, Left, ChR2 stimulation evoked monosynaptic EPSC, followed by polysynaptic EPSCs, presumably because of parallel fiber activity caused by activation of descending input to granule cells. Right, 50-Hz ChR2 stimulation evoked numerous small EPSCs that cannot be individually resolved. The EPSCs were AMPAR-mediated, as they were blocked by GYKI53655. Recorded in the presence of 50 $\mu$M 4-AP. ***C***, This cell was in a caudal section of DCN containing mostly the molecular layer. Z-projection. A second tdTomato-labeled cartwheel cell is visible in the boxed region. ***D***, Magnified view of boxed region in ***C***. Biocytin-labeled cartwheel cell. Z-projection.

mediated outward currents in OFF UBCs require a train of synaptic stimulation and were not accompanied by phasic EPSCs, we were unable to confirm the monosynaptic nature of these inputs based on latency. Thus, these cells are not included in Table 1. However, both OFF UBCs had ChR2-Venus-labeled axonal contacts onto their dendritic brushes, which provides an anatomical demonstration of direct input from descending IC axons (Fig. 2*J*). In sum, although the descending IC projections are glutamatergic, they excite ON UBCs and inhibit OFF UBCs, according to the receptor subtypes in the postsynaptic cells.

### Granule cells and Golgi cells receive descending input from IC

Granule cells are numerous in regions surrounding DCN and are known to receive multiple inputs from extrinsic nonauditory sources as well as from the IC (Caicedo and Herbert, 1993). However, their postsynaptic responses to descending IC input have not been reported. Granule cells can be identified by their small soma diameter (5–7 µm) and high input resistance (>800 MΩ; Fig. 4*A*). Optogenetic activation of descending IC inputs caused phasic EPSCs in granule cells that could drive action potential firing and could reliably follow input at 50 Hz (Fig. 4*B*,*C*). In this example, a 1-ms light pulse evoked a −57.3-pA EPSC with a latency of 1.66 ms with a 97% success rate. The EPSCs were mediated by AMPA receptors, as they were blocked by GYKI53655 (50 $\mu$M; Fig. 4*D*). This granule cell was in the region between DCN and VCN and received bouton-like contacts onto rather simple dendrites (Fig. 4*E*–*G*). Unlike in the cerebellum, granule cells in the DCN often do not have "claw-like" dendrites (Mugnaini et al., 1980), as in this example. Mossy fiber-like contacts were observed in other examples (Fig. 4*H*,*I*). Of the nine granule cells that had ChR2-evoked EPSCs, five were filled with biocytin and imaged. Three additional examples are shown in Figure 5. All of the imaged cells had evidence of a ChR2-Venus-labeled axon in close apposition to one of the recorded cell's dendrites, providing anatomical evidence that the synaptic currents were the result of monosynaptic input from axons arising from IC. Thus, granule cells may process auditory input from the IC, in addition to nonauditory input.

Golgi cells receive multisensory input from extrinsic sources and are the sole inhibitory neuron of the granule cell domain, and provide feed-forward and feed-back inhibition to granule cells (Yaeger and Trussell, 2015) and make electrical synaptic contacts between one another (Yaeger and Trussell, 2016). In this dataset, we were able to identify and record from only one Golgi cell that received direct input from IC. Golgi cells are the largest cells in the granule cell regions and can be identified electrophysiologically by their low input resistance and regular firing (Fig. 6*A*). Optogenetic stimulation of IC axons caused AMPA receptor-mediated EPSCs that facilitated (Fig. 6*B*) during repetitive activity. The illustrated Golgi cell was recovered and had a large (~20 µm) diameter soma and processes extending for hundreds of micrometers in every direction (Fig. 6*C*,*D*), some of which were closely apposed with labeled descending axons (Fig. 6*E*). Consistent with Golgi cells being excited by optogenetic activation of IC input, in recordings from some UBCs and granule cells disynaptic (long-latency) IPSCs were evoked by ChR2 activation, and these were blocked by the glycine receptor antagonist strychnine (0.5 $\mu$M, $n = 2$). Thus, all the major cell types of the granule cell domain receive direct, glutamatergic input from the ipsilateral IC.

### Cell types outside of the granule cell domains also receive descending IC input

There are at least four cell types outside of the granule cell domain, including vertical, cartwheel, principal cells and superficial stellate cells. To our surprise, we were able to find definitive examples of IC input to all these cell types, with the exception of the superficial stellate cells.

Vertical cells (also called tuberculoventral cells) are glycinergic interneurons that receive auditory nerve input and provide feedforward inhibition to principal neurons, sharpening the principal neuron responses to a given frequency of acoustic signal (Rhode, 1999; Davis and Young, 2000). We recorded and recovered nine vertical cells, which can be identified electrophysiologically by their high-frequency firing (Kuo et al., 2012; Fig, 7*A*). Optogenetic stimulation of descending IC fibers evoked fast-decaying EPSCs that were mediated by AMPA receptors. In this example both monosynaptic and disynaptic EPSCs are apparent (Fig. 7*B*). In five vertical cells that were tested, 2 could be driven to fire action potentials with a train of light pulses. Vertical cells lie in the deep layer and have a narrow dendritic field that lie along an isofrequency band (Fig. 7*C*,*D*). Inhibitory vertical cells also project ventrally and could therefore transmit descending IC signals to VCN. In all cases tested, the EPSCs were blocked by GYKI ($n = 5$).

Cartwheel cells also inhibit the principal cells of the DCN. Their excitatory input is thought to be multimodal, as they are

excited by the parallel fiber axons of granule cells. Cartwheel cells are easy to identify by their complex spiking behavior in which a series of $Na^+$ spikes "ride" on a slow $Ca^{2+}$-mediated depolarization (Fig. 8*A*). Optogenetic stimulation of descending IC axons caused a short-latency, monosynaptic response, followed by a slow disynaptic response; we interpret these profiles to reflect direct input from IC, followed by feedforward excitation through the granule cells (Fig. 8*B*). Upon recovery of the biocytin filled cell there were two cartwheel cells in the same region that were both transynaptically labeled with tdTomato (Fig. 8*C*, boxed region). The cartwheel cell that was filled with biocytin during the whole-cell recordings shown in Figure 8*A*,*B* had two dendrites and a well-labeled axon that extended in the region of one of the dendrites (Fig. 8*D*). Interestingly, cartwheel cells have been reported to respond to sound in some *in vivo* experiments, but no auditory nerve inputs have been seen anatomically (Portfors and Roberts, 2007). It is therefore possible that cartwheel cells receive their auditory information from IC through the connections identified here. It is likely that these neurons do not receive input from the same parallel fibers as the fusiform cells that they inhibit (Roberts and Trussell, 2010), and thus could provide lateral inhibition to inhibit some fusiform cells in favor of others, thereby gating transmission of specific sound frequencies in DCN.

In some respects, the most striking observation of this study is that the principal neurons of the DCN, fusiform cells and giant cells, also responded to optogenetic activation of fibers originating in the IC. Their responses were both monosynaptic and disynaptic, indicating direct contact from IC and feedforward excitation from granule cells. In the illustrated example, the duration of the LED pulse to activate the fibers was adjusted to activate monosynaptic EPSCs (0.1-ms duration) or both monosynaptic and disynaptic inputs (4-ms duration). These EPSCs were blocked by GYKI and were therefore mediated by AMPARs in all cells tested ($n = 3$). Five of the six principal cells that had electrophysiological evidence of input from IC were recovered. In order to provide convincing evidence for this pathway from IC projection neuron to DCN projection neuron, we illustrate all five examples in Figures 9, 10. While the size and location of these neurons strongly indicates they are principal cells, precise identification as fusiform versus giant cell is difficult. Since these neurons have the IC as their sole synaptic target, our results reveal a novel, direct feedback loop to the brainstem.

Superficial stellate cells, which lie in the molecular layer of DCN among the parallel fibers, were not confirmed to be transsynaptically labeled in these experiments. The descending fibers from IC are not present in the molecular layer, which agrees with that lack of trans-synaptic labeling and supports the conclusion that superficial stellate cells do not receive input from the IC.

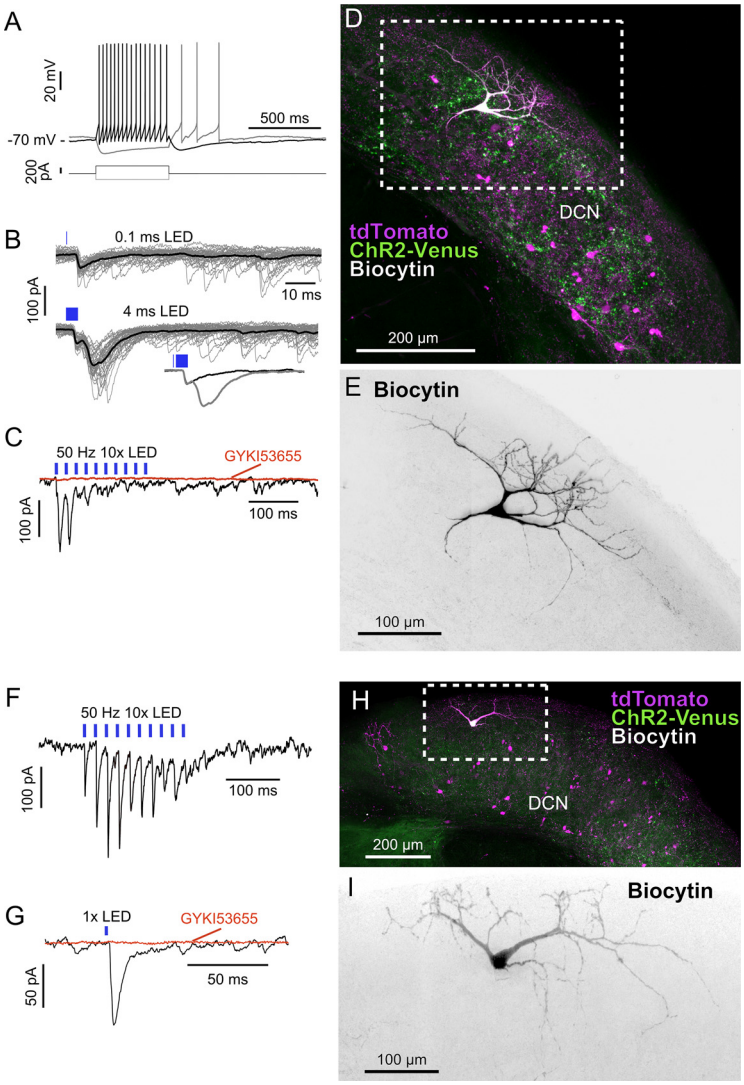


**Figure 9.** Principal cells are excited by descending IC axons. ***A***, Hyperpolarizing and depolarizing current steps. The regular spiking pattern is consistent with that of a fusiform cell. ***B***, Top, 0.1-ms light pulses evoked a monosynaptic EPSC. Bottom, 4-ms light pulses evoked both monosynaptic and polysynaptic EPSCs. Inset, The averages evoked by 0.1- and 4-ms duration light pulses overlaid and aligned to the first EPSC shows that the monosynaptic EPSCs are of similar amplitude and shape, although they appeared with a shorter latency in response to the longer duration stimulation (2.4 vs 3.0 ms). Recorded in the presence of 50 $\mu$M 4-AP. ***C***, The EPSC was entirely AMPAR-mediated, being completely blocked by GYKI53655. Recorded in the presence of 50 $\mu$M 4-AP. ***D***, Large cell with soma in the fusiform cell layer and dendrites in both the molecular and deep layers. Z-projection. ***E***, Magnified view of boxed region in ***D***. Biocytin-labeled fusiform cell. Z-projection. ***F***, 50-Hz ChR2 stimulation evoked EPSCs that were quite different from the responses of the other targets of descending inputs, having a "build-up" inward current and facilitation followed by depression. Recorded in the presence of 50 $\mu$M 4-AP. ***G***, The EPSC was entirely AMPAR-mediated, being completely blocked by GYKI53655. Recorded in the presence of 50 $\mu$M 4-AP. ***H***, This cell's dendrites spanned a width of the molecular layer, making it unlikely to be a fusiform cell or a cartwheel cell. To our knowledge, only giant cells are this large. Giant cell somata are typically deeper, but all other characteristics match the giant cell type. Z-projection. ***I***, Magnified view of boxed region in ***H***. Biocytin-labeled giant cell. Z-projection.

## Discussion

The descending IC projection to DCN targets all the cell types in the granule cell domain (granule cells, ON UBC, OFF UBCs, Golgi cells) as well as vertical cells, cartwheel cells and principal cells (fusiform or giant cells), but not superficial stellate cells (Fig. 11). All of the projections are glutamatergic and excite cells

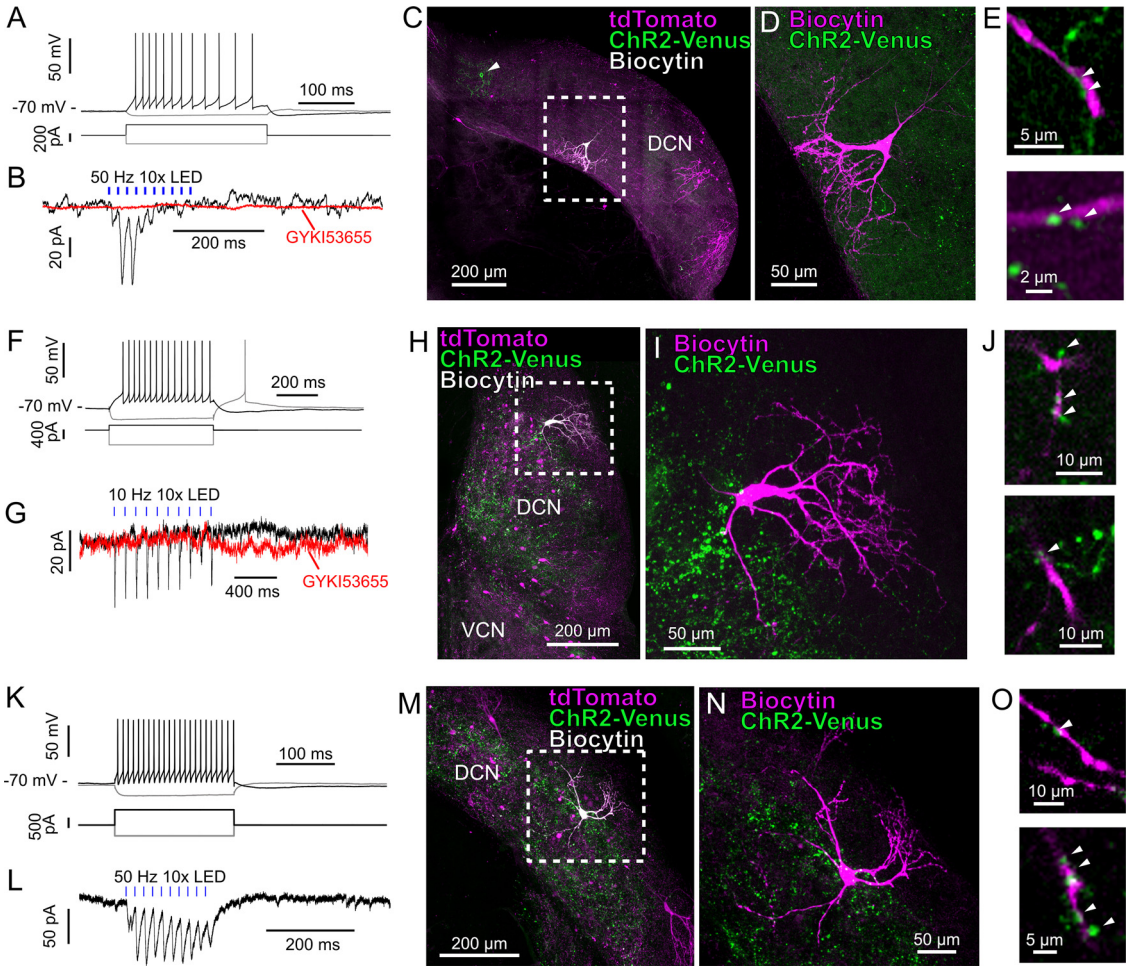


**Figure 10.** Additional examples of principal cells with anatomically and functionally defined connections. ***A***, Regular spiking in response to depolarizing current step. ***B***, Average EPSCs evoked by 50-Hz train of LED pulses. The first several LED pulses were more likely to evoke an EPSC than later pulses. The evoked and spontaneous EPSCs were blocked by AMPA receptor antagonist GYKI53655 (50 $\mu$M). There were many failures and the latency of the EPSCs were difficult to measure because of high-frequency spontaneous EPSCs. The average latency to the foot of the first evoked EPSC was 3.70 ms. These currents were recorded in the presence of 50 $\mu$M 4-AP. ***C***, This caudal section of DCN contained primarily molecular layer, thus accounting for the apparent mis-orientation of the fusiform cell. Note the single ChR2-Venus-expressing cell in the medial part of DCN indicated by arrowhead. This is the sole example of a DCN neuron that expressed ChR2-Venus. Z-projection. ***D***, Expanded view of boxed region in ***C***. Z-projection. ***E***, Examples of contacts between the biocytin filled dendrite and ChR2-Venus-labeled fibers. Single optical planes. ***A–E*** from one cell. ***F***, Spiking pattern is consistent with principal cell type. ***G***, 10-Hz LED stimulation evokes EPSCs that were blocked by GYKI53655. The average latency of the first EPSC was 2.29 ms. These currents were recorded in the presence of 50 $\mu$M 4-AP. ***H***, Biocytin filled principal cell in DCN. Z-projection. ***I***, Higher magnification view of the boxed region in ***H***. Z-projection. ***J***, Close contact between ChR2-Venus-labeled axons and biocytin filled basal dendrites. Single optical planes. ***F–J*** from one cell. ***K***, Regular spiking response to current step. ***L***, 50-Hz ChR2 stimulation evoked train of EPSCs. The average latency of the first EPSC was 3.41 ms. These currents were recorded in the presence of 50 $\mu$M 4-AP. ***M***, Another example principal cell that was filled with biocytin during whole-cell recording. Z-projection. ***N***, Expanded view of boxed region in ***M***. Z-projection. ***O***, Putative contacts between ChR2-Venus-labeled axon and biocytin filled basal dendrite. Single optical planes. ***K–O*** from one cell.

via AMPA receptors, except in the case of OFF UBCs, in which glutamate also evokes long-lasting IPSCs through mGluR2 receptors. The synaptic targeting reported here provides neural substrates for diverse network effects including: (1) increasing or decreasing parallel fiber activity (via ON UBCs and OFF UBCs or Golgi cells); (2) exciting principal cells directly or indirectly (via the parallel fiber pathway); (3) inhibiting principal cells indirectly through either vertical or cartwheel cells; and (4) inhibiting VCN neurons through vertical cells. The breadth of the feedback projection from IC has not been fully appreciated and could be involved in complex auditory mechanisms. As we conducted our study in mice from P27 to P40, it is possible that the projections we identified could change in size and diversity with age.

The trans-synaptic labeling approach allowed us to target postsynaptic neurons for recording and was essential for the discovery that nearly all cell types of the DCN receive descending glutamatergic input from IC. This unbiased approach revealed unknown projections that could have important roles in hearing. One difficulty with this approach is that the AAV1-Syn-Cre virus infects axons as well, and therefore cannot be used for projections that are reciprocally connected. However, this approach is appropriate for the IC-DCN projection because DCN projects almost entirely to the contralateral IC, and IC projects many more axons to ipsilateral DCN. Because the two sides of IC are so strongly connected by commissural fibers (Saldaña and Merchán, 1992), the descending ipsilateral IC projection likely carries information that is integrated across hemispheres. In theory, the strong interconnections across the two ICs may make bilateral descending projections unnecessary. On the other hand, the descending projection may provide information from the contralateral ear that could contribute to binaural acoustic processing in DCN.

### Descending glutamatergic input rapidly inhibits OFF UBCs

The main response of OFF UBCs to synaptic glutamate is to pause their spontaneous firing, because of their strong mGluR2-

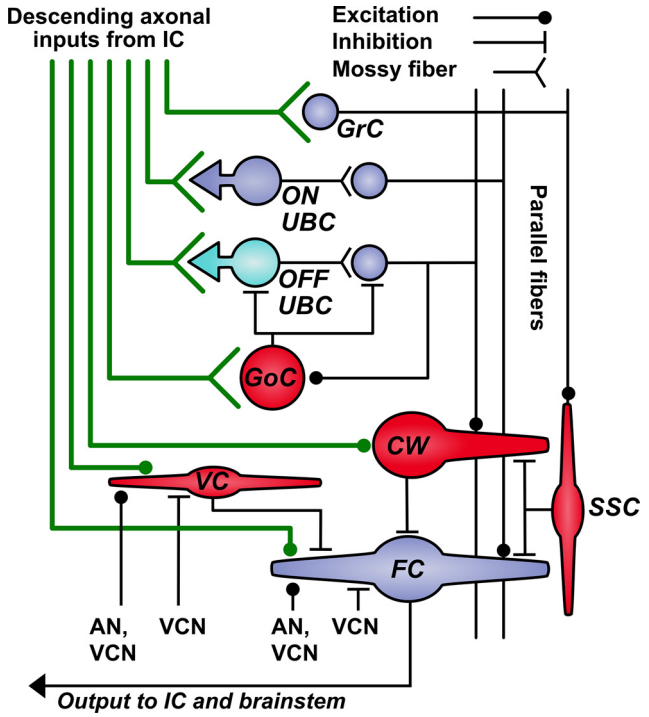


**Figure 11.** Inputs to cell types of the DCN and granule cell domains. Extrinsic inputs from IC are marked in green. Other extrinsic or intrinsic inputs labeled as black lines. Nonauditory extrinsic inputs are omitted for clarity. AN: auditory nerve; CW: cartwheel cell; FC: fusiform/giant cell; GoC: Golgi cell; GrC: granule cell; OFF UBC: OFF subtype of UBC; ON UBC: ON subtype of UBC; SSC: superficial stellate cell; VC: Vertical cell; VCN: ventral cochlear nucleus.

mediated hyperpolarization (Borges-Merjane and Trussell, 2015). Thus, this descending input, though glutamatergic, has an inhibitory effect on OFF UBCs. A pause in OFF UBC activity would reduce parallel fiber activity and the excitation of principal cells and cartwheel cells. This is an unconventional circuit motif that converts a glutamatergic signal to an inhibitory one more directly than a circuit that utilizes an inhibitory interneuron, which would necessarily slow the signal because of synaptic delays. Thus, the OFF UBC may be specialized to rapidly reduce parallel fiber activity in response to top-down signals. A similar mechanism was recently identified in the vestibular cerebellum, in which OFF UBCs of the cerebellar cortex receive glutamatergic input from fibers originating in the medial vestibular nucleus (Balmer and Trussell, 2019).

### Role of descending auditory projections in hearing

The IC is a nearly obligate auditory processing area and its descending fibers could therefore refine how signals are processed at the earliest level of auditory processing in the brain. For example, top-down auditory signals from IC could excite principal neurons that respond to specific frequencies to improve the detection of specific sounds, bringing only those cells closer to spike threshold, and enhancing their sensitivity to bottom-up auditory nerve signals. By contrast, descending projections to vertical cells could act as a frequency filter, inhibiting specific frequency regions of the tonotopic axis. Central gain enhancement through top-down signaling could compensate for hearing damage at specific frequencies and contribute to the hidden hearing loss phenomenon in which significant deafferentation occurs before clinical hearing loss can be detected (Liberman and Kujawa, 2017).

These proposed mechanisms depend on the assumption that descending input from IC is tonotopically organized (Milinkeviciute et al., 2017). However, the axons of auditory granule cells (parallel fibers) run along the DCN's tonotopic axis, and so it is hard to see how such frequency-specific input could be preserved for the effects of auditory input to the granule cell domain. Against this concern is the possibility that, while the granule cell axons cross tonotopic bands, their influence may still be spatially restricted. Indeed, parallel fiber axons of the cerebellum may not make synaptic contacts continuously along their length, but instead target specific bands of functionally related Purkinje cells (Valera et al., 2016). Thus, in principle, descending auditory signals to granule cells, and to UBCs, could lead to selective enhancement of activity in principal cells. Alternatively, descending input to the granule cell domain, perhaps in concert with nonauditory input, could increase (through granule cells and ON UBCs) and decrease (through OFF UBCs and Golgi cells) the excitability of the auditory input domain cells in unison for a nonfrequency specific enhancement or suppression.

### Role of descending multisensory projections in hearing

Inputs from IC may convey nonauditory "multisensory" signals and could be one of the main sources of multisensory input to DCN to underlie functions such as cancellation of self-generated sounds. The IC is a major hub of multisensory integration, processing axonal inputs from somatosensory, visual and auditory cortices (Cooper and Young, 1976; Olthof et al., 2019), and somatosensory brainstem nuclei (Tokunaga et al., 1984; Paloff and Usunoff, 1992). The cell types in the granule cell region are known to process extrinsic nonauditory signals from regions of various modalities, and the relative balance among these contributions is unclear (Ryugo et al., 2003). The signals from IC may differ, however, in that they could carry a signal already integrated across multiple sensory modalities including audition. These truly "multimodal" signals could provide the DCN necessary information for sound source localization based on combined cues arising from the somatosensory, visual and auditory systems. Whether multisensory signals are indeed carried by IC projections and whether they target cell types according to the information they carry remains to be addressed by conducting *in vivo* experiments.

### Potential role for descending IC-DCN projection in tinnitus

The DCN is thought to be a prominent locus in the maintenance of tinnitus, the perception of an ongoing subjective sound (Kaltenbach and Godfrey, 2019). Accordingly, the presence of feedback to DCN could underlie mechanisms involved in tinnitus or its correction. For example, the descending excitatory feedback is likely to be tonotopic (Milinkeviciute et al., 2017) and could underlie tinnitus that is associated with hearing loss at the same frequency (König et al., 2006; Moore et al., 2010; Zhou et al., 2011) by causing a frequency-specific prediction error. For example, descending input could convey a prediction of the acoustic environment that includes frequencies no longer being encoded by the bottom-up auditory nerve signals because of cochlear damage or deafferentation. That mismatch could lead to an imbalance that causes a frequency-specific hyperactivity, leading to the perception of a frequency not present.

Modeling suggests that lateral inhibition could underlie enhanced activity at the point of the tonotopic axis where

hearing loss is present, because the region adjacent to the damaged frequency are disinhibited (Gerken, 1996). Our finding that the IC projects directly to inhibitory interneurons that underlie lateral inhibition of neighboring frequencies suggests that this top-down feedback has the potential to correct the disinhibition and thus could suppress tinnitus. Indeed, hearing loss often occurs without tinnitus and perhaps top-down mechanisms could underlie this dissociation.

## References


Andersen RA, Roth GL, Aitkin LM, Merzenich MM (1980) The efferent projections of the central nucleus and the pericentral nucleus of the inferior colliculus in the cat. J Comp Neurol 194:649–662.

Balmer TS, Trussell LO (2019) Selective targeting of unipolar brush cell subtypes by cerebellar mossy fibers. Elife 8:e44964.

Benson TE, Berglund AM, Brown MC (1996) Synaptic input to cochlear nucleus dendrites that receive medial olivocochlear synapses. J Comp Neurol 365:27–41.

Borges-Merjane C, Trussell LO (2015) ON and OFF unipolar brush cells transform multisensory inputs to the auditory system. Neuron 85:1029–1042.

Caicedo A, Herbert H (1993) Topography of descending projections from the inferior colliculus to auditory brainstem nuclei in the rat. J Comp Neurol 328:377–392.

Conlee JW, Kane ES (1982) Descending projections from the inferior colliculus to the dorsal cochlear nucleus in the cat: an autoradiographic study. Neuroscience 7:161–178.

Cooper MH, Young PA (1976) Cortical projections to the inferior colliculus of the cat. Exp Neurol 51:488–502.

Davis KA, Young ED (2000) Pharmacological evidence of inhibitory and disinhibitory neuronal circuits in dorsal cochlear nucleus. J Neurophysiol 83:926–940.

Faye-Lund H (1986) Projection from the inferior colliculus to the superior olivary complex in the albino rat. Anat Embryol (Berl) 175:35–52.

Feliciano M, Saldaña E, Mugnaini E (1995) Direct projections from the rat primary auditory neocortex to nucleus sagulum, paralemniscal regions, superior olivary complex and cochlear nuclei. Aud Neurosci 1:287–308.

Gerken GM (1996) Central tinnitus and lateral inhibition: an auditory brainstem model. Hear Res 97:75–83.

Gustafsson MG (2000) Surpassing the lateral resolution limit by a factor of two using structured illumination microscopy. J Microsc 198:82–87.

Guzman SJ, Schlögl A, Schmidt-Hieber C (2014) Stimfit: quantifying electrophysiological data with Python. Front Neuroinform 8:16.

Kaltenbach JA, Godfrey DA (2019) The cochlear nucleus as a generator of tinnitus-related signals. In: The Oxford handbook of the auditory brainstem (Kandler K, ed), pp 188–222. Oxford: Oxford University Press.

Kandler K, Schofield BR, Beebe NL (2018) Descending auditory pathways and plasticity. In: The Oxford handbook of the auditory brainstem (Kandler K, ed). Oxford: Oxford University Press.

König O, Schaette R, Kempter R, Gross M (2006) Course of hearing loss and occurrence of tinnitus. Hear Res 221:59–64.

Kuo SP, Lu HW, Trussell LO (2012) Intrinsic and synaptic properties of vertical cells of the mouse dorsal cochlear nucleus. J Neurophysiol 108:1186–1198.

Liberman MC, Kujawa SG (2017) Cochlear synaptopathy in acquired sensorineural hearing loss: manifestations and mechanisms. Hear Res 349:138–147.

Madisen L, Mao T, Koch H, Zhuo JM, Berenyi A, Fujisawa S, Hsu YW, Garcia AJ 3rd, Gu X, Zanella S, Kidney J, Gu H, Mao Y, Hooks BM, Boyden ES, Buzsáki G, Ramirez JM, Jones AR, Svoboda K, Han X, et al. (2012) A toolbox of Cre-dependent optogenetic transgenic mice for light-induced activation and silencing. Nat Neurosci 15:793–802.

Malmierca MS, Le Beau FE, Rees A (1996) The topographical organization of descending projections from the central nucleus of the inferior colliculus in guinea pig. Hear Res 93:167–180.

Meltzer NE, Ryugo DK (2006) Projections from auditory cortex to cochlear nucleus: a comparative analysis of rat and mouse. Anat Rec A Discov Mol Cell Evol Biol 288:397–408.

Milinkeviciute G, Muniak MA, Ryugo DK (2017) Descending projections from the inferior colliculus to the dorsal cochlear nucleus are excitatory. J Comp Neurol 525:773–793.

Moore BC, Vinay, Sandhya (2010) The relationship between tinnitus pitch and the edge frequency of the audiogram in individuals with hearing impairment and tonal tinnitus. Hear Res 261:51–56.

Mugnaini E, Warr WB, Osen KK (1980) Distribution and light microscopic features of granule cells in the cochlear nuclei of cat, rat, and mouse. J Comp Neurol 191:581–606.

Olthof BM, Rees A, Gartside SE (2019) Multiple non-auditory cortical regions innervate the auditory midbrain. J Neurosci 39:8916–8928.

Paloff AM, Usunoff KG (1992) Projections to the inferior colliculus from the dorsal column nuclei. An experimental electron microscopic study in the cat. J Hirnforsch 33:597–610.

Petreanu L, Huber D, Sobczyk A, Svoboda K (2007) Channelrhodopsin-2-assisted circuit mapping of long-range callosal projections. Nat Neurosci 10:663–668.

Petreanu L, Mao T, Sternson SM, Svoboda K (2009) The subcellular organization of neocortical excitatory connections. Nature 457:1142–1145.

Portfors CV, Roberts PD (2007) Temporal and frequency characteristics of cartwheel cells in the dorsal cochlear nucleus of the awake mouse. J Neurophysiol 98:744–756.

Roberts MT, Trussell LO (2010) Molecular layer inhibitory interneurons provide feedforward and lateral inhibition in the dorsal cochlear nucleus. J Neurophysiol 104:2462–2473.

Rhode WS (1999) Vertical cell responses to sound in cat dorsal cochlear nucleus. J Neurophysiol 82:1019–1032.

Rossi DJ, Alford S, Mugnaini E, Slater NT (1995) Properties of transmission at a giant glutamatergic synapse in cerebellum: the mossy fiber-unipolar brush cell synapse. J Neurophysiol 74:24–42.

Ryugo DK, Haenggeli CA, Doucet JR (2003) Multimodal inputs to the granule cell domain of the cochlear nucleus. Exp Brain Res 153:477–485.

Saldaña E, Merchán MA (1992) Intrinsic and commissural connections of the rat inferior colliculus. J Comp Neurol 319:417–437.

Schofield BR (2002) Ascending and descending projections from the superior olivary complex in guinea pigs: different cells project to the cochlear nucleus and the inferior colliculus. J Comp Neurol 453:217–225.

Singla S, Dempsey C, Warren R, Enikolopov AG, Sawtell NB (2017) A cerebellum-like circuit in the auditory system cancels responses to self-generated sounds. Nat Neurosci 20:943–950.

Tokunaga A, Sugita S, Otani K (1984) Auditory and non-auditory subcortical afferents to the inferior colliculus in the rat. J Hirnforsch 25:461–472.

Valera AM, Binda F, Pawlowski SA, Dupont J-L, Casella J-F, Rothstein JD, Poulain B, Isope P (2016) Stereotyped spatial patterns of functional synaptic connectivity in the cerebellar cortex. Elife 5:e09862.

Weedman DL, Ryugo DK (1996) Projections from auditory cortex to the cochlear nucleus in rats: synapses on granule cell dendrites. J Comp Neurol 371:311–324.

Yaeger DB, Trussell LO (2015) Single granule cells excite Golgi cells and evoke feedback inhibition in the cochlear nucleus. J Neurosci 35:4741–4750.

Yaeger DB, Trussell LO (2016) Auditory Golgi cells are interconnected predominantly by electrical synapses. J Neurophysiol 116:540–551.

Zhou X, Henin S, Long GR, Parra LC (2011) Impaired cochlear function correlates with the presence of tinnitus and its estimated spectral profile. Hear Res 277:107–116.

Zingg B, Chou XL, Zhang ZG, Mesik L, Liang F, Tao HW, Zhang LI (2017) AAV-mediated anterograde transsynaptic tagging: mapping corticocollicular input-defined neural pathways for defense behaviors. Neuron 93:33–47.

Zingg B, Peng B, Huang J, Tao HW, Zhang LI (2020) Synaptic specificity and application of anterograde transsynaptic AAV for probing neural circuitry. J Neurosci 40:3250–3267.